Development of an automated diode-laser-based multicomponent gas sensor

Dirk Richter, David G. Lancaster, and Frank K. Tittel

The implementation and application of a portable fiber-coupled trace-gas sensor for the detection of several trace gases, including CO_2, CH_4, and H_2CO, are reported. This particular sensor is based on a cw fiber-amplified near-infrared (distributed Bragg reflector) diode laser and an external cavity diode laser that are frequency converted in a periodically poled lithium niobate crystal to the mid-IR spectroscopic fingerprint region (3.3–4.4 μm). A continuous absorption spectrum of CH_4 and H_2CO from 3.37 to 3.70 μm with a spectral resolution of 40 MHz (~0.0013 cm^{-1}) demonstrated the spectral performance that can be achieved by means of automated wavelength tuning and phase matching with stepper motor control. Autonomous long-term detection of ambient CO_2 and CH_4 over a 3- and 7-day period was also demonstrated. © 2000 Optical Society of America

OCIS codes: 190.2620, 300.6340.

1. Introduction

The spectroscopic detection and quantification of numerous trace-gas species has become an important aspect in many industrial, urban, and environmental applications. More importantly, there is a need to selectively detect several different molecular gas species simultaneously by means of a single, tunable, and portable sensing device capable of high sensitivity and rapid response time.

Characteristic absorption bands of most molecules can be found in the near-infrared (overtone) and mid-infrared (fundamental rovibrational) spectral region. The latter range has the advantage that the spectrum is less congested and exhibits ~20–200 times stronger absorption cross sections. Established techniques for multicomponent gas analysis include nonlaser-based Fourier-transform infrared spectrometers that can rapidly cover a broad spectrum (~1 s) with a typical resolution of 15 GHz.[1] For highly selective (~50-MHz) absorption spectroscopy of trace gases, various narrow-linewidth laser sources are used in the mid-IR, including cw cyrogenically cooled lead–salt diode lasers[2–4] and, more recently, cw and pulsed quantum cascade lasers.[5] In the near-IR spectral region, room-temperature operation of cw single or multisection distributed feedback InGaAsP diode lasers can be applied to overtone absorption spectroscopy.[6] An alternative, narrow-linewidth mid-IR spectroscopic source that has been applied successfully to trace-gas detection is based on difference-frequency generation (DFG) of two near-IR diode lasers in a nonlinear optical material such as periodically poled lithium niobate (PPLN).[7–9]

In this paper we describe the development and application of an automated mid-IR diode-laser-pumped DFG-based trace-gas sensor source that offers wide tunability from 3.3 to 4.4 μm and a spectral selectivity of ~40 MHz. A fiber-coupled tunable near-IR external cavity diode laser (ECDL) (814–870 nm) and a Yb-fiber-amplified distributed Bragg reflector (DBR) diode-laser (1083 nm) are used as DFG pump sources. The two pump lasers are difference-frequency mixed in a fan-out-type PPLN crystal that offers high optical conversion efficiency, broad spectral transmission (0.3–5.3 μm), and continuous quasi-phase matching. This sensor uses extractive, direct absorption spectroscopy at a reduced pressure (~80 Torr) in a multiple-pass absorption cell fitted with astigmatic mirrors (18 or 36 m).[10] Several gases including CH_4, CO_2, $H^{35,37}Cl$, H_2CO, N_2O, NO_2, CH_3OH, and C_6H_6 have been detected to date within the tuning range of this DFG-based gas sensor. Spectral tuning and quasi-phase matching by means of stepper motors are controlled by LabView software operating on a laptop PC and interfaced

The authors are with the Rice Quantum Institute, Rice University, Houston, Texas 77251-1892. The e-mail address for F. K. Tittel is fkt@rice.edu.

Received 4 January 2000; revised manuscript received 24 May 2000.

0003-6935/00/244444-07$15.00/0

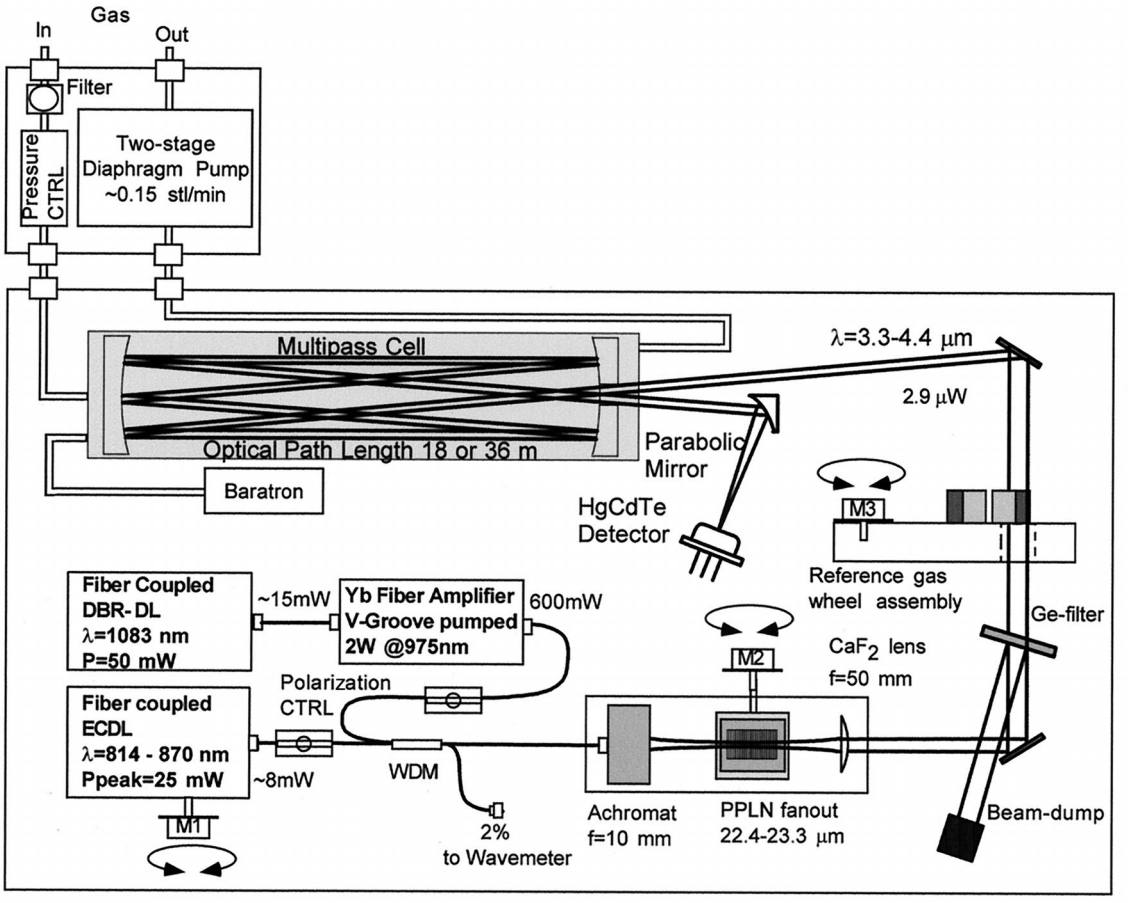

Fig. 1. Schematic of an automated DFG multicomponent gas sensor. M1, M2, and M3 are stepper motors for the ECDL, PPLN crystal stage, and reference gas assembly, respectively. WDM, wavelength division multiplexer; DL, diode laser; CTRL, control.

with serial ports. Furthermore, the fast measurement response time of typically 5–10 s, including averaging and automated data processing, allows the real-time monitoring of *in situ* and remote chemical and atmospheric trace-gas species.

2. Gas Sensor Configuration

The gas sensor developed for field operation utilizes both a fiber-pigtailed, widely tunable 25-mW ECDL operating at a center wavelength of 842 ± 28 nm and a fiber-pigtailed 50-mW DBR diode laser operating at a 1083-nm wavelength (see Fig. 1). Continuous, mode-hop-free tuning of the Littman-type ECDL is selected by simultaneous rotation and translational movement of the internal feedback mirror about a pivot point with respect to the grating by means of a linear translation stage.[11] This linear translation stage was modified to implement a stepper motor and was operated by use of a compact computer-controlled driver. The fiber-coupled output power of ~15 mW from the DBR diode laser was amplified to 600 mW by a side-pumped Yb fiber amplifier using a 2-W diode laser at 975 nm.[12,13] Both ECDL and amplified DBR diode-laser fiber-coupled beams pass through polarization controllers before being combined by use of a four-port fiber coupler. Two percent of the combined beam power was connected to a second fiber coupler, separating the pump and signal beams. Either optical fiber arm can be connected to a wavemeter for absolute frequency calibration. For convenience, the ECDL beam was monitored continuously with the wavemeter (precision: $\pm 0.01\ \mathrm{cm}^{-1}$ at $\lambda = 1\ \mu\mathrm{m}$) to provide absolute frequency tuning information by a general-purpose interface bus (GPIB) Personal Computer Memory Card International Association (PCMCIA) interface. Alternatively, a solid etalon in combination with a silicon photodiode could be used as a relative wavelength tuning reference.[14] The other 98% are terminated in an 8-deg angle-polished fiber connector and mounted onto a ruggedized DFG conversion stage. This stage contains the optical elements and optomechanical mounts that are pertinent to achieve widely tunable DFG, including a fiber port, imaging lens, PPLN crystal, and a CaF_2 lens. We imaged the collinear pump beams from the fiber tip into the temperature-controlled antireflection-coated PPLN crystal using an $f = 10$-mm achromatic lens. A kinematic optical mount with vertical translation and tilt is used to align the crystal to the beam propagation axis. This mount is also controlled by a stepper-motor-driven linear translation stage to provide the optimal quasi-phase-matching grating period. The dialing position is computed from an experimentally

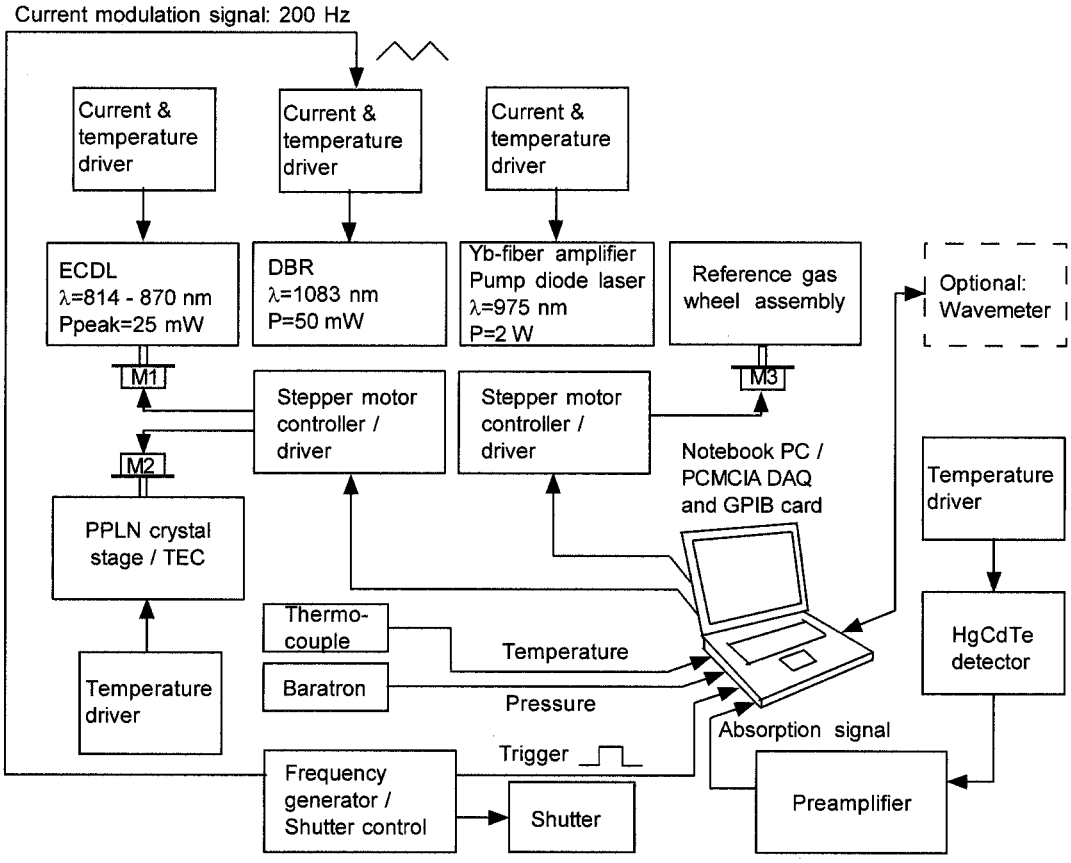

Fig. 2. Diagram of the electronic control and data-acquisition system for the DFG-based multicomponent gas sensor. DAQ, data acquisition; TEC, thermoelectric cooler.

recorded phase-matching function. Both the single-mode fiber-launched pump and the signal beams possess Gaussian beam profiles, and when mixed in a 19-mm-long PPLN crystal they produce a diffraction-limited mid-IR DFG beam of ~2.9-μW power at ~3.5-μm wavelength.[8] The DFG beam is then collimated by use of an $f = 50$-mm CaF_2 lens, passing through a Ge filter to block the unconverted pump beams and directed to a multipass cell (physical length, ~30 cm; actual path length, 18 or 36 m).[10] The sensor operated with a typical sensitivity of 2×10^{-4} limited by the occurrence of etalon effects introduced by the optical elements. For convenient identification and tracking specific absorption line center positions within the scan width, up to five individual reference gas cells ($L = 5$ cm) can be rotated into the DFG beam path by a stepper-motor-driven assembly. The sensor is also operated and controlled with a LabView software code running on the laptop PC. Figure 2 shows the electronic diagram of the gas sensor. Both stepper motor controllers are interfaced to the laptop PC by a universal serial bus port. A 16-bit PCMCIA data-acquisition card is used to acquire the absorption signal synchronized to a trigger signal, the gas sampling pressure, and temperature. The card also controls a shutter through a digital transistor–transistor logic line for background light subtraction that is necessary for an absolute spectroscopic absorption measurement. The entire sensor, including both optical and electronic elements, is packaged into a suitcase with outside dimensions of 61 cm × 53 cm × 20 cm. An additional small suitcase (30 cm × 25 cm × 14 cm) contains a diaphragm pump and a mass-flow controller that are used for extractive gas sampling at reduced pressure for optimum spectral selectivity and sensitivity.

3. Wavelength Tuning and Quasi-Phase-Matching Characteristics

The wavelength tuning curve for the Littman-type external cavity pump laser as a function of the stepper motor rotation (dial position) is shown in Fig. 3. A miniature coupler from the stepper motor shaft to the ECDL tuning screw was used. This coupler permitted angular, radial, and lateral misalignment of the stepper motor shaft and therefore suppressed stress to the ECDL tuning mechanism. The stepper motor resolution was 1/3600 steps per revolution and provided an experimentally measured linear ECDL frequency tuning rate of 0.018 cm^{-1}/step. The frequency tuning was superimposed by a sinusoidallike modulation, corresponding to a peak deviation of 0.15 cm^{-1} as can be seen from the inset of Fig. 3. This inset also shows a residual backlash of 225 ± 15 steps inherent to the ECDL device used in this research.

Continuous quasi-phase matching over the entire

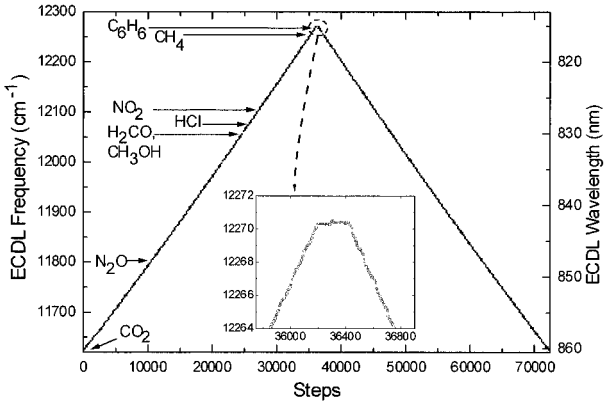

Fig. 3. ECDL frequency tuning characteristic with stepper motor control.

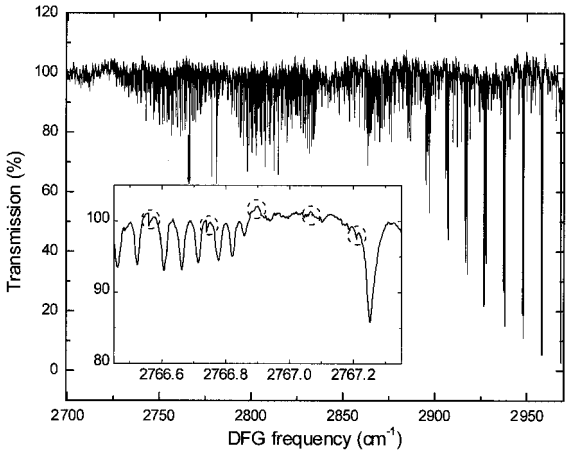

Fig. 5. Measured absorption spectra of formaldehyde and methane over 270 cm^{-1} centered at 2850 cm^{-1}. Estimated total pressure was 50 Torr (8% CH_4 and 0.65% H_2CO); absorption path length was 5 cm.

tuning range of the sensor is achieved by use of a PPLN crystal with a fan-out grating structure.[15] In this configuration the grating period continuously increases from 22.4 to 23.3 μm over a 1-cm-wide crystal. Plotted in Fig. 4 is the relative crystal position versus the DFG wavelength for two temperatures, 26 °C and 44 °C. The PPLN crystal temperature can be set to match the available grating periods with the ECDL wavelength tuning range, which for this sensor is 44 °C. For comparison, a multichannel PPLN crystal (common channel period spacing of 0.1 μm) requires a temperature adjustment to optimally phase match intermediate wavelengths. For example, for a pump–signal–idler wavelength combination, which requires a grating period that lies between two nominal PPLN crystal channel grating periods of 0.1-μm difference, a temperature adjustment of ±15 °C is necessary.[8,16] The measured PPLN phase-matching bandwidth is 28 cm^{-1} (Fig. 4). This value can be compared with a theoretically computed phase-matching bandwidth of 12.5 cm^{-1} at 3.6 μm for normal-incidence nondiverging pump beams. Similar to the ECDL stepper motor interface, a miniature joint coupling was used to connect to the PPLN crystal linear translation stage (Vernier set screw, 0.5-mm linear translation per revolution). In addition, a 48-pitch, 1:1 Miter gear was implemented to realize a compact stepper motor arrangement with no noticeable loss of precision.

The simultaneous computer control of wavelength tuning and quasi-phase matching allows multispecies gas measurements within the instrument tuning range from 3.3 to 4.4 μm. For example, Fig. 5 shows a continuous absorption spectra of methane (CH_4) and formaldehyde (H_2CO) acquired over a 270-cm^{-1}-

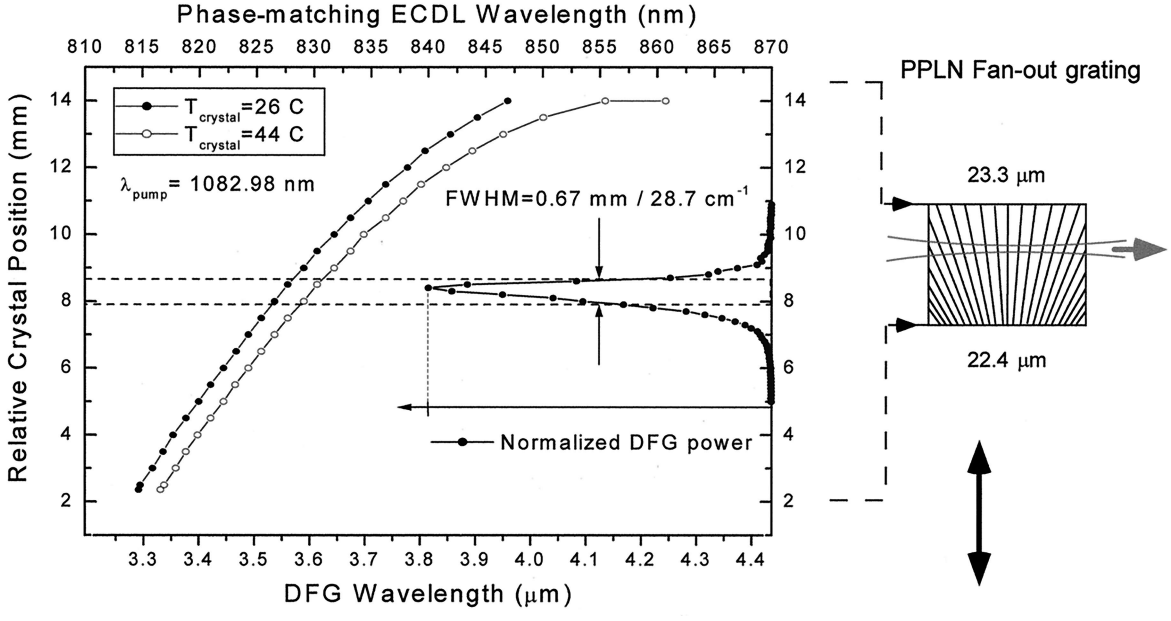

Fig. 4. Continuous quasi-phase matching with a fan-out grating-type PPLN crystal.

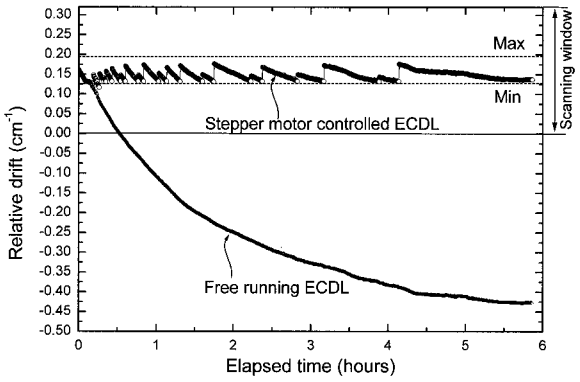

Fig. 6. Comparison of the relative frequency drift for a stepper-motor-controlled and free-running ECDL operation as a function of time.

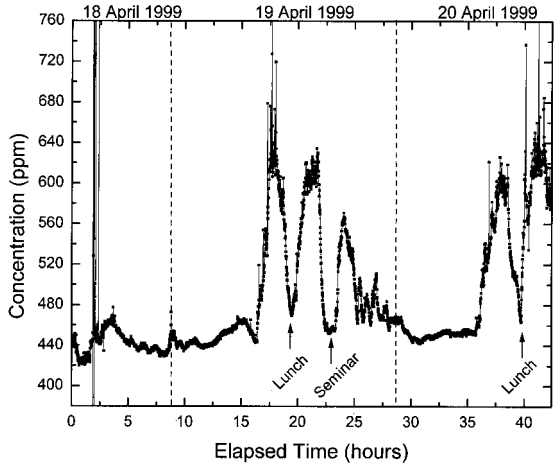

Fig. 7. Ambient CO_2 laboratory sampling over a 42-h time period.

wide tuning range from 2700 cm^{-1} (3.70 μm) to 2970 cm^{-1} (3.37 μm) with a DFG linewidth resolution of 40 MHz. We performed the measurement using a 5-cm-long reference gas cell containing 8% of CH_4 and 0.65% of H_2CO with an estimated total pressure of 50 Torr. A 200-Hz current modulation of the DBR diode laser provided an effective scanning width of 0.33 cm^{-1}. The ECDL was tuned consecutively by an eight-step ($\sim$0.15-cm^{-1}) increment to take into account the above-mentioned sinusoidal offset. Absolute wavelength accuracy was provided by a wavemeter. Each spectrum was averaged over five scans (25 ms) and subtracted by a five-scan average dark voltage measurement to obtain absolute transmission. The recorded spectroscopic data files that include an absorption scan, dark voltage scan, and corresponding wavelength log were automatically processed with a LabView software-programmed algorithm to connect the acquired spectra (indicated by the dashed circles in the inset of Fig. 5) and to remove redundant data points of consecutive data scans. Furthermore, a polynomial-fit algorithm can be applied to improve the baseline overlap of two consecutive scans.

Automated compensation of wavelength drift that is due to temperature changes is a further advantage of our using stepper-motor-controlled wavelength tuning and quasi-phase matching. Critical components that are susceptible to temperature fluctuations include detector amplifier, diode-laser drivers, temperature controllers, and, most significantly, the wavelength stability of the ECDL. Figure 6 shows an example of automated wavelength drift compensation by means of the two stepper motors. For this measurement the absorption peak location of a CO_2 transition line at $\sim$4.2 μm was monitored after the DFG-based gas sensor was moved from an outdoor to an indoor environment with an ambient temperature difference of $\sim$5 °C. At the beginning of the measurement the absorption line was centered within the absorption scan width of 0.32 cm^{-1}. We programmed the LabView software to compensate for the drift of the absorption by appropriately wavelength tuning the ECDL if the peak location was outside the programmed maximum and minimum boundary conditions. For comparison, the total wavelength drift that can occur if the gas sensor system is not actively controlled is also shown in Fig. 6.

4. Spectroscopic Evaluation of the Difference-Frequency Generation-Based Gas Sensor

The DFG-based gas sensor was used in several long-term tests. In a first test, the sensor was tuned to a CO_2 line at 2385.77 cm^{-1} (4.2 μm) and monitored the CO_2 concentration in ambient laboratory air continuously at reduced pressure of 80 Torr for a 3-day period as depicted in Fig. 7. The rovibrational CO_2 absorption lines at $\sim$4.2 μm have a frequency spacing of $\sim$0.7 cm^{-1} (21 GHz). In this case, it is advantageous to perform spectroscopic absorption measurements of CO_2 at a reduced sampling pressure to avoid a zero baseline offset. The CO_2 concentration increases and decreases rapidly, respectively, at times with and without human activity in the laboratory as shown in Fig. 7. The dynamic detection range at this CO_2 absorption line is 0.5–2200 parts per million (ppm) (100% absorption) at a pressure of 80 Torr for an 18-m optical absorption path-length-configured multipass cell and a residual optical noise of 2×10^{-4}. After 2 h into the CO_2 sampling test, human breath was briefly sampled and caused a sharp increase to CO_2 levels of more than 2200 ppm, saturating the absorption signal. However, it is possible to tune the DFG wavelength to a weaker CO_2 transition to measure higher concentrations or to lower frequencies to access a stronger CO_2 transition at 4.2 μm when low CO_2 concentrations are measured. The DFG-based gas sensor measured higher ambient background levels than the atmospheric concentrations measured by the National Oceanic and Atmospheric Administration.[17] This may be due to the fact that the CO_2 and other gas species concentration levels tend to be higher in urban areas such as Houston, Texas.

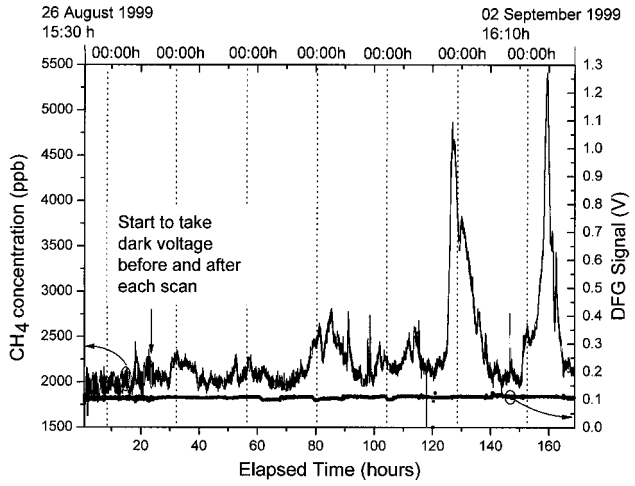

Fig. 8. Continuous detection of ambient CH_4 for a 7-day period.

In another long-term test, the DFG sensor was tuned to a methane absorption line at 3028.751 cm^{-1} (3.3 μm) to monitor ambient air continuously for a 7-day period. The DFG-based gas sensor was located in an air-conditioned laboratory environment with the sensor being located close to an air-conditioner ventilation inlet. For this test, the multipass cell was aligned to a 36-m optical path configuration for increased detection sensitivity. Approximately 20 min into the test, the DFG-based gas sensor was set to acquire a dark voltage before and after each absorption scan and to compute an average absorption value. This effectively reduces the noise present in a CH_4 measurement evident in Fig. 8. Furthermore, one can see that the methane concentration peaks around midnight and increased to over 5000 parts per billion (ppb) after heavy rain storms. These methane trends were confirmed to be real by an intercomparison with another fiber-coupled DFG-based gas sensor.[18] At the bottom of Fig. 8 the corresponding DFG output power signal is plotted. A general drift of 0.03%/h with a 1.3% standard deviation is measured, except of a few incidents when a cooling fan attached to the Yb fiber amplifier housing stopped operation. This effectively changed the temperature-dependent pump diode wavelength which resulted in a shift to a weaker absorption cross-section region of the Yb-doped fiber amplifier and led to a reduced amplifier gain.

A second CH_4 sensor, described in Ref. 18, was set up in close vicinity and operated at the same DFG wavelength and measured ambient laboratory air with a 36-m open path-length multipass cell at atmospheric pressure. Figure 9 shows the superimposed CH_4 concentration measurements versus time plots of the two independently operating DFG-based trace-gas sensors over a 4-day period. Both sensors fol-

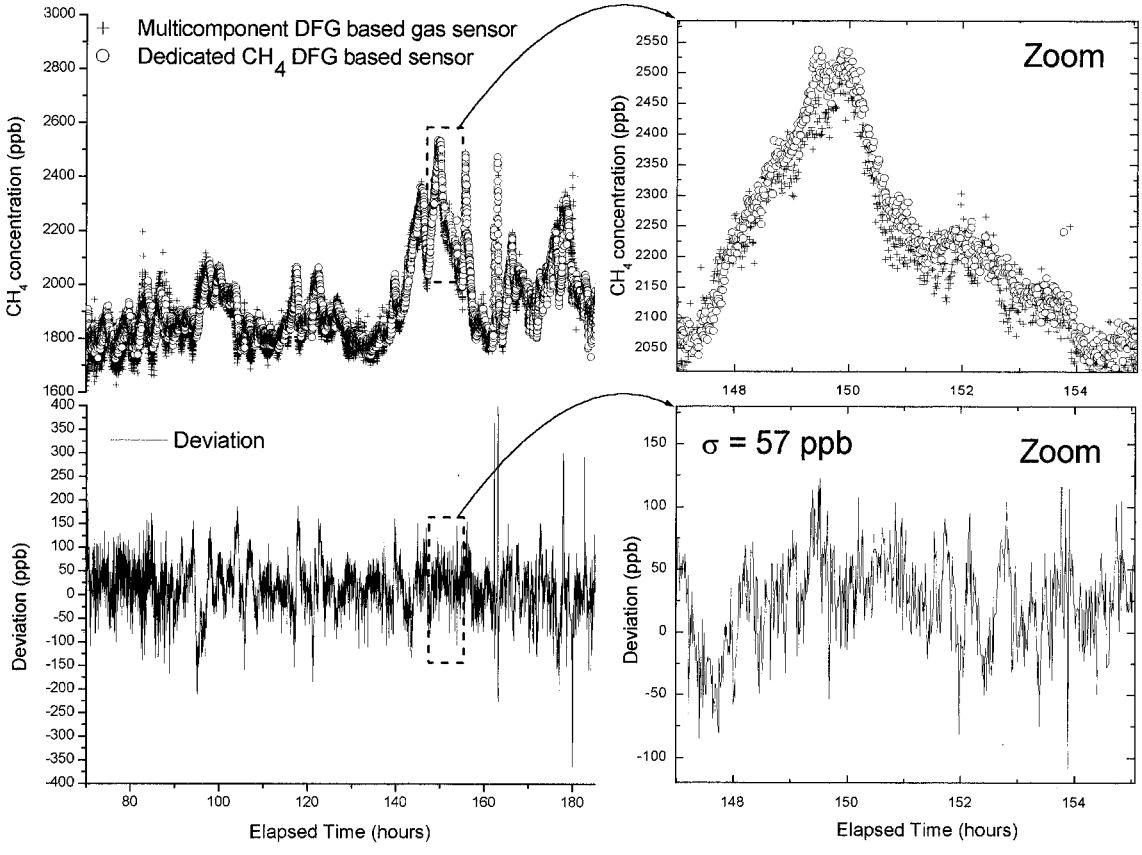

Fig. 9. Intercomparison of long-term CH_4 concentration measurements by two independent DFG-based gas sensors indicating both CH_4 concentrations and deviation in parts per billion.

lowed the same profile and measured the CH_4 concentration with an average difference of 50 ppb (standard deviation), which is well within the accuracy of both instruments (5%). For calibration of the DFG-based gas sensors, a calibrated gas mixture was flown through the multipass cells.[8] Using LabView software, we first processed the absorption scans to obtain a flat baseline, and then we fitted the absorption signal to a Lorentzian line-shape function using a nonlinear least-squares Levenberg–Marquardt fit.[8] The obtained spectroscopic parameters also agree with the HITRAN[19] database. Furthermore, the good agreement between atmospheric and low sampling pressure (88 Torr) measurements indicates a high spectral purity of the two DFG-based gas sensors and confirms the applicability of a Lorentzian line-shape function.

5. Summary

We reported the development and application of a portable, compact, widely tunable mid-IR DFG-based gas sensor that can be operated automatically with stepper motor wavelength tuning and continuous PPLN quasi-phase matching. Fiber optics and fiber-coupled diode-laser pump sources make such a device suitable for nonlaboratory use of gas sensing applications. Long-term monitoring of CO_2 and CH_4 and the acquisition of a continuous CH_4 and H_2CO absorption spectra over 270 cm^{-1} further demonstrates the key advantages of this DFG-based gas sensor, including robust long-term maintenance-free operation and wide tunability for multicomponent gas detection with high sensitivity, selectivity, and real-time response.

To achieve better sensitivity, more power is required to apply advanced detection techniques such as dual-beam detection to effectively cancel out the occurrence of optical etalon effects.[20] Potentially, the same sensor architecture also can be used to access the second atmospheric window from 6 to 16 μm with orientation-patterned epitaxial-grown quasi-phase-matched GaAs crystal for optical frequency conversion.[21]

The authors acknowledge D. P. Leleux (Rice University) for the support and help in implementing the stepper motor control hardware and software. Financial support was provided by NASA, the Texas Advanced Technology Program, the Welch Foundation, the National Science Foundation, and the Gulf Coast Hazardous Substance Research Center.

References and Notes

1. Midac Corporation, 17911 Fitch Ave., Irvine, Calif. 92614; http://www.midac.com.
2. A. Fried, B. Henry, B. Wert, S. Sewell, and J. R. Drummond, "Laboratory, ground-based, and airborne tunable diode laser systems: performance characteristics and applications in atmospheric studies," Appl. Phys. B **67,** 317–330 (1998).
3. D. D. Nelson, M. S. Zahniser, J. B. McManus, C. E. Kolb, and J. L. Jiménez, "A tunable diode laser system for the remote sensing of on-road vehicle emissions," Appl. Phys. B **67,** 433–441 (1998).
4. P. Werle, "A review of recent advances in semiconductor laser based gas monitors," Spectrochim. Acta Part A **54,** 197–236 (1998).
5. F. Capasso, C. Gmachl, D. L. Sivco, and A. Y. Cho, "Quantum cascade lasers," Phys. World **12,** 27–33 (1999).
6. B. L. Upschulte, D. M. Sonnenfroh, and M. G. Allen, "Measurements of CO, CO_2, OH, and H_2O in room temperature and combustion gases by use of a broadly current-tuned multisection InGaAsP diode laser," Appl. Opt. **38,** 1506–1512 (1999).
7. D. Richter, D. G. Lancaster, R. F. Curl, W. Neu, and F. K. Tittel, "Compact mid-infrared trace gas sensor based on difference frequency generation of two diode lasers in periodically poled $LiNbO_3$," Appl. Phys. B **67,** 347–350 (1998).
8. D. G. Lancaster, D. Richter, and F. K. Tittel, "Portable fiber coupled diode laser based sensor for multiple trace gas detection," Appl. Phys. B **69,** 459–465 (1999).
9. M. Seiter and M. W. Sigrist, "On-line multicomponent trace-gas analysis with a broadly tunable pulsed difference frequency laser spectrometer," Appl. Opt. **38,** 4691–4698 (1999).
10. J. B. McManus, P. L. Kebabian, and M. S. Zahniser, "Astigmatic mirror multipass absorption cells for long-path-length spectroscopy," Appl. Opt. **34,** 3336–3348 (1995).
11. R. J. Lang, D. G. Mehuys, and D. F. Welch, "External cavity, continuously tunable wavelength source," U.S. patent, 5,771,252 (23 June 1998).
12. J. P. Koplow, L. Goldberg, and D. A. V. Kliner, "Compact 1-W Yb-doped double-cladding fiber amplifier using V-groove side pumping," IEEE Photon. Technol. Lett. **10,** 793–795 (1998).
13. L. Goldberg, B. Cole, and E. Snitzer, "V-groove side pumped 1.5 μm fibre amplifier," Electron. Lett. **33,** 2127–2129 (1997).
14. K. W. Aniolek, T. J. Kulp, B. A. Richman, S. E. Bisson, P. E. Powers, and R. L. Schmitt, "Trace gas detection in the mid-IR with a compact PPLN-based cavity ring-down spectrometer," in *Application of Tunable Diode and Other Infrared Sources for Atmospheric Studies and Industrial Processing Monitoring II*, A. Fried, ed., Proc. SPIE **3758,** 62–73 (1999).
15. P. E. Powers, T. J. Kulp, and S. E. Bisson, "Continuous tuning of continuous-wave periodically poled lithium niobate optical parametric oscillator by use of a fan-out grating design," Opt. Lett. **23,** 159–161 (1998).
16. D. H. Jundt, "Temperature-dependent Sellmeier equation for the index of refraction, n_e, in congruent lithium niobate," Opt. Lett. **22,** 1553–1555 (1997).
17. National Oceanic and Atmospheric Administration (NOAA), Climate Monitoring and Diagnostics Laboratory (CMDL), Carbon Cycle Group, http://www.cmdl.noaa.gov/ccgg.
18. D. G. Lancaster, R. Weidner, D. Richter, F. K. Tittel, and J. Limpert, "Compact CH_4 sensor based on difference frequency mixing of diode lasers in quasi-phase matched $LiNbO_3$," Opt. Commun. **175,** 461–468 (2000).
19. L. S. Rothman, R. R. Gamache, A. Goldman, L. R. Brown, R. A. Toth, H. M. Pickett, R. L. Poynter, J.-M. Flaud, C. Camy-Peyret, A. Barbe, N. Husson, C. P. Rinsland, and M. A. H. Smith, "The HITRAN database: 1986 edition," Appl. Opt. **26,** 4058–4097 (1987).
20. D. G. Lancaster, A. Fried, B. Wert, B. Henry, and F. K. Tittel, "Difference-frequency-based tunable absorption spectrometer for detection of atmospheric formaldehyde," Appl. Opt. **39,** 4436–4443 (2000).
21. L. A. Eyres, P. J. Tourreau, T. J. Pinguet, C. B. Ebert, J. S. Harris, M. M. Fejer, B. Gerard, and E. Lallier, "Quasi-phase matched frequency conversion in all-epitaxial, orientation patterned 200-μm-thick GaAs films," Stanford University Annual Report 1998–1999 (Center for Nonlinear Optical Materials, Stanford University, Stanford, Calif., 1999), pp. 37–41.